International Journal of Innovative Technology and Exploring Engineering (IJITEE)
ISSN: 2278-3075 (Online), Volume-9 Issue-3, January 2020

Potential Application of Hough Transform to Extract Hot Spot Delineated Boundaries Using Landsat-8 Satellite Images

Tasneem Ahmed, Mohammad Usama

Abstract*: Coal fires, also known as subsurface fires or hot spots are all-inclusive issues in coal mines everywhere throughout the globe. Aimless mining over a period of past 100 years has prompted large scale damages to the ecosystem of the earth. For example, debasement in nature of water, soil, air, vegetation dissemination and variations in land topography have caused degradation. Research is needed to be more attentive on developing the prospective use of the satellite image analysis for hot spot detection because ground-based hot spots monitoring is time-taking, complex, cumbrous and very expensive. In this paper, a two-stage model has been developed to extract the hot spot delineated boundaries in Jharia coal field (JCF) region. In the first stage, contextual thresholding (CT) technique has been used to classify the hot spot and non-hot spot regions. After thorough processing, hot spots regions have been retrieved and for performance evaluation sensitivity and specificity are calculated, which suggest that hot spots were detected accurately in successful and efficient way. In second stage, the Canny edge detection algorithm is applied to detect the edges of the hot spot regions and then the binary image is generated, which is later converted into a vector image. Finally Hough transform is implemented on the obtained vector images for delineating hot spot boundaries. In future, delineated hot spot boundaries may be used to obtain the expansion or shrinking information of hot spot regions and it can be used for area estimation also.

Keywords: Hot Spot, Contextual Thresholding, Hough Transform, Sensitivity, Specificity, Edge Detection and Boundary Delineation.

I. INTRODUCTION

Subsurface coal fires are serious threat to natural resources and cause environmental degradation such as water, soil, and air pollution, changes in topography, land use/ land cover and vegetation patterns [1]. Satellite images offer help in the identification and detection of the hot spots which has resulted in better understanding of the changes occurring within the environment that leads to counter action within the time-frame.

Revised Manuscript Received on January 30, 2020.
***** Correspondence Author
Tasneem Ahmed*, Department of Computer Application, Integral University, Lucknow, India. Email: tasneemfca@iul.ac.in
Mohammd Usama, Department of Environmental Science, Integral University, Lucknow, India. Email: mdusama@iul.ac.in

This kind of information may be retrieved and investigated for land use monitoring from processed satellite images by utilizing the existing image segmentation technique like image thresholding, because image segmentation process provides the precise and accurate segregation of the objects and also provide the characterization of very small objects.

A brief review on the applications of various satellite images in hot spot identification and detection techniques is given in [2], where it is noticed that many researchers have used optical and TM data for surface or subsurface coal fire monitoring. It is also observed that various optical satellite images such as Landsat-TM [3]–[6], Moderate Resolution Imaging Spectroradiometer (MODIS) [7], [8], and National Oceanic and Atmospheric Administration's Advanced Very High Resolution Radiometer (NOAA/AVHRR) etc. [9]–[12], have been used for coal fire monitoring. Recently, a burned forest areas mapping on Landsat-TM images have been presented by Chen et al. in 2016 [13] and it is realized that Landsat-TM allows a more objective and accurate understanding of the losses caused by that fire. Detection of coal fires using multispectral thermal images such as Landsat-TM and SPOT-5 images have been discussed in [14], which may be viewed as an application of satellite images for the detection of coal fires.

Many researchers have used various techniques for hot spot monitoring with satellite images such as principal component analysis (PCA) with information fusion, fuzzy logic, contextual thresholding model, image stacking, support vector machine (SVM) and wavelet transform based model [9]–[11], [15], [16]. However, there is still uncertainty about the problem of hot spot monitoring and the most important aspect behind subsurface fire monitoring is to monitor their expansion and contractility by delineating the boundaries of hot spot regions. In a brief literature review, it is observed that satellite images have been used for object detection and object identification. It is also noticed that, during the extraction of some important features like structural information and characteristics etc., it is necessary to remove the unwanted background data from the image, which could be done through edge detection [17]. Since the output image retrieved from an edge detector is defined as an image by its pixels, the removal of unwanted data could be more specific if ellipses and lines are defined by their characteristic equations. Hough transform is basically used to retrieve the rectangular and circular shaped building boundaries [17],

in which the original image is classified by using some classification method to separate the background and building pixels. In this present work, Hough transform is used to retrieve the lines and arbitrary shapes of hot spot regions. Initially, an image containing JCF region is classified to separate the hot spot regions from non-hot spot regions by using contextual thresholding (CT) technique. The results obtained from each image are estimated in terms of the hot spot detection accuracy (HDA) and false alarm rate (FAR). Later, the edge detection technique is applied to the classified image to retrieve the edges of the hot spot regions. After that, the Hough transform is applied to obtain the boundaries of the hot spot regions.

The remaining paper is arranged as follows. In the next section, a brief description of the satellite data and study region used in this study is discussed. Section 3 contains the theoretical background of pre-processing of Landsat images, physical significance of normalized difference vegetation index (NDVI), and a short description about Hough transform and then development of model for detecting hot spots. Following that, Section 4 presents a discussion on the result retrieved from the CT by measuring the HDA and FAR. After that Section 5 presents a discussion on the implementation of Hough transform on two class classified images for edge detection, boundary delineation, and performance evaluation of delineated hot spot boundaries. Finally, the last section contains the concluding remarks.

II. STUDY AREA AND SATELLITE DATA USED

A. Study Area

Jharia Coal Field (JCF) region has been taken as the study area, which is located in the heart of the Damodar Valley and is about 250 km northwest of Kolkata and 1150 km southeast of Delhi. It lies between latitudes 22000'N and 24000'N and longitude 85000E and 87000E. Fig, 1, shows the Geological map of Jharia Coal Field region.

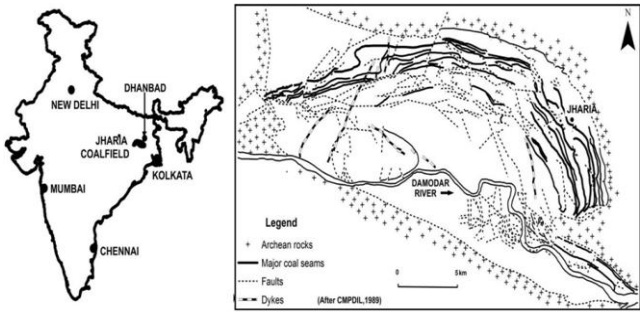

Fig. 1. Geological map of Jharia Coal Field region[18]

B. Satellite Data Used

Landsat-8 images from January 2015 to June 2015 have been incorporated in this study. Landsat-8 images consist of eleven spectral bands with a spatial resolution of 30 meters for bands 1-7, and 9, 15 meters for band-8, while bands 10 and 11 (thermal bands) are of 100 meters. Satellite images details with acquisition ID and acquisition Dates are shown in Table-I, where Data ID has been given the name as IMG_01 to IMG_06 to all the images for further use.

Table- I: Landsat-8 satellite images used for the study

Sl. No.	Acquisition ID	Acquisition Date	Data ID
1.	LC81400442015017LGN00	17/01/2015	IMG_01
2.	LC81400432015033LGN00	02/02/2015	IMG_02
3.	LC81400432015081LGN00	22/03/2015	IMG_03
4.	LC81400442015097LGN00	09/04/2015	IMG_04
5.	LC81400442015129LGN00	11/05/2015	IMG_05
6.	LC81400442015161LGN00	10/06/2015	IMG_06

III. THEORITICAL BACKGROUND AND IMPLEMENTATION

There are various satellite images with different spatial resolutions and with multiple spectral bands characteristics. Resolution defines the level of Earth's surface information that can be distinguished from it, while pixel is the smallest unit in the satellite image which represents the spatial resolution and Earth's surface area. For hot spot monitoring, it is observed that Near Infrared (NIR) is the most appropriate spectral band for optical images, because the hot spot regions are generally characterized by a low reflection in response to underground fire due to the loss of vegetation in the NIR band, disappearance of groundwater and existence of ash and charcoal [19], [20]. Therefore, to detect the coal mining areas, a good quality satellite image is required having a fine spatial resolution and multiple spectral bands characteristics. Hence, Landsat-8 satellite images are the most commonly used images for hot spot detection because it consists of eleven spectral bands and also provide fine spatial resolution with multiple spectral images for better and efficient hot spot monitoring. Therefore, in this paper Landsat-8 satellite images are utilized to detect the subsurface hot spots.

A. Pre-processing of Landsat-8 Images

Landsat-8 images are already Geo-coded and surface reflectance values are presented by digital numbers. Radiometric Calibration of Landsat-8 images has been done in ENVI 5.1 to retrieve the surface reflectance values by converting the digital numbers to the reflectance. For each month image, normalized difference vegetation index (NDVI) image has been calculated by using the Red (620-670 nm) and Near Infrared (841-876 nm) bands and their projection has been converted from UTM to Geographic Latitude and Longitude.

B. Calculation of NDVI

Normalized difference vegetation index (NDVI) is one of the most commonly used vegetation index for measuring the greenness and vegetation abundance over a region. It helps to distinguish between the green vegetation and soil brightness. It is a ratio image formed by the composite of NIR and Red bands which is mathematically expressed in "(1)".

$$\mathrm{NDVI} = \frac{(\rho_{NIR} - \rho_{Red})}{(\rho_{NIR} + \rho_{Red})} \qquad (1)$$

The NDVI value falls within the range of -1 to +1. Positive NDVI refers to the presence of vegetation while negative refers to the presence of water bodies or non-vegetated areas.

NDVI value falling around zero is a physical sign of the presence of bare soil ground or rock.

It is observed that NDVI plays an important role in the detection of a hot spot due to the fact that hot spot region usually has bare ground such that neither bushes nor grasses grow over or nearby the hot spot region.

C. Hough Transform

Hough Transform was patented by Paul Hough in 1962, which is a method to detect curves by exploiting multiple points on a curve. It is used for extracting the line of an arbitrary curve. If edge detector is compared with Hough transform, the former one defines only where features are in an image while that of later one is to determine both what the features are and how many of them exist in a particular image [21]. The Hough transform converts a complex problem of detecting a shape in image space into a problem of peak detection [22] which is quite easier. When Hough transform is applied on an image, the detected lines of the arbitrary curve is transformed into the binary form i.e. voting number, coordinate of two pixels of a straight line and its angle [23]. In other words, Hough transformation for straight lines is actually point-to-curve transformation. An excellent feature of this transform technique is that it will also work even when the boundary is not connected either due to noise or blockage. Since Hough transform treats each and every point independently, parallel processing of all points is possible. Therefore this transform technique can be extended to detect shapes such as road, wall, building, beach, pipe, underground cable, underwater tracking and lane detection in parking [17], [24].

$$y = a.x + b \qquad (2)$$

$$b = -a.x + y \qquad (3)$$

However, in Fig. 2 it is noticed that the above form is not able to represent vertical lines.

Now, on the other hand, we have convenient equations for describing a set of lines which uses either parametric or normal notion as shown in "(4)" and "(5)":

$$r = x.\cos\theta + y.\sin\theta \qquad (4)$$

$$y = -\frac{\cos\theta}{\sin\theta}.x + \frac{r}{\sin\theta} \qquad (5)$$

where r represents the length and θ (theta) is an angle from the origin of a normal to the line as the transformation from line to the Hough space depicted in Fig. 2.

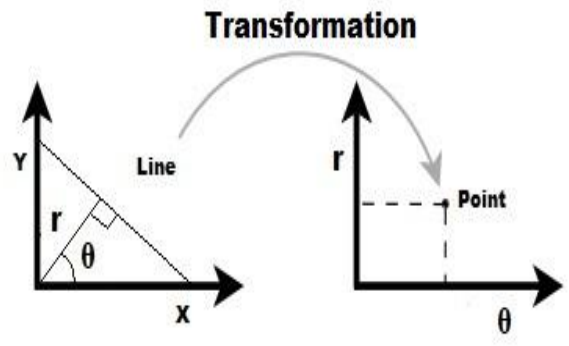

Fig. 2. A transformation from line to the Hough space

IV. MODEL DEVELOPMENT AND IMPLEMENTATION FOR HOT SPOT DETECTION

Landsat-8 image of March 2015 (i.e. IMG_03 has given in Table-I) has been taken to classify the hot spot and non-hot spot pixels by applying the CT algorithm on a subset of JCF region. Fig. 3 shows the flow chart of the proposed model, where dotted lines show the hot spot classification and hot spot delineation after implementing the Hough transform.

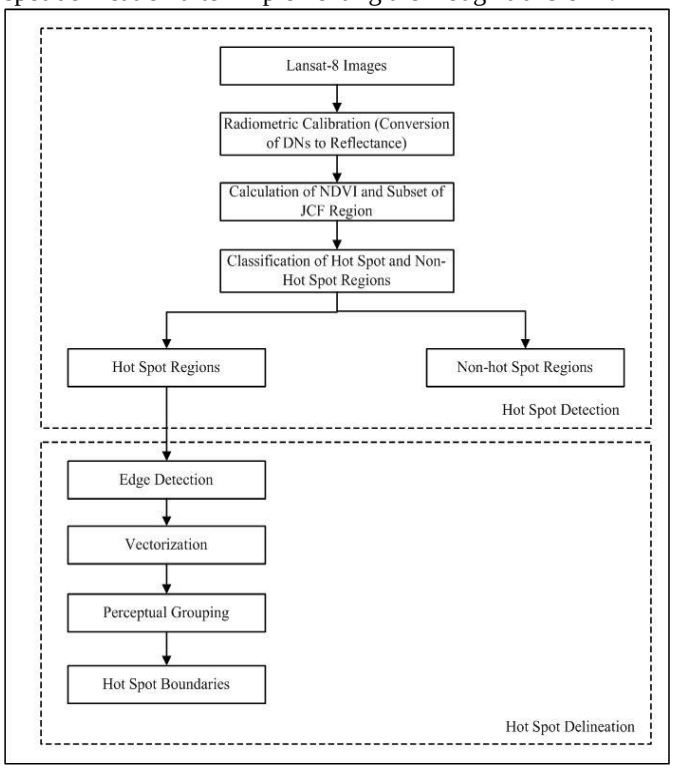

Fig. 3. Flowchart of hot spot detection and hot spot boundary delineation

After segregating the hot spot and non-hot spot regions, the background pixels (non-hot spot regions) are excluded from the image. Before applying the Hough transform, the edge detection algorithm has been used to obtain the edges and the edges detected image is retrieved as the binary image which illustrate the edges of the hot spot regions. Then Hough transform is applied to the binary image to transform it into the vector form. Later, to obtain the hot spot boundaries, the detected lines or curves in the vector form are grouped perceptually.

V. RESULTS AND DISCUSSIONS

All the 6 images (i.e. IMG_01 to IMG_06 as given in Table-I) of Landsat-8 data are pre-processed individually and radiometric calibration has been applied to obtain the surface reflectance values over the JCF region. Their projection has been changed from UTM to Geographic Latitude and Longitude and a subset of the JCF region has been taken for further processing.

A. Pre-processing of Landsat-8 Images

After obtaining the surface reflectance values over the JCF region, IMG_03 image is taken for development purpose.

January and February month's images (i.e. IMG_01 and IMG_02) are used for algorithm testing, while April, May and June month's images (i.e. IMG_04, IMG_05, and IMG_06) are used for algorithm validation purpose. NDVI image is calculated from IMG_03 by using the "(1)" and it is retrieved as NDVI_03 and shown in Fig. 4.

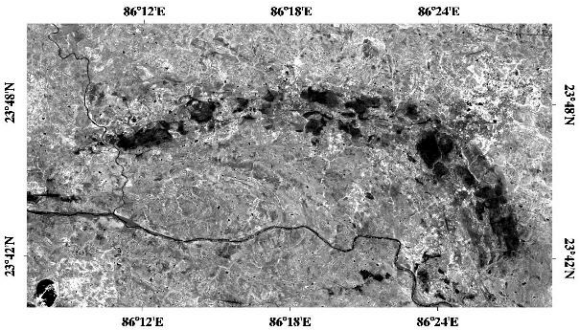

Fig. 4. NDVI images of JCF region (i.e. NDVI_03)

NDVI could be useful for hot spot detection because it is observed that the possibility of vegetation will be very less over the hot spot regions. From Fig. 4, it is observed that hot spot and non-hot spot regions have been enhanced by computing the NDVI of the JCF region. The enhanced hot spot regions are observed as dark pixels and non-hot spot region as bright pixels, but to extract the exact hot spot and non-hot spot pixels, there is need to apply the thresholding algorithm.

B. Contextual Thresholding (CT) based Classification of Hot Spot and Non-hot Spot Regions

To obtain the two class classified image of the hot spot and non-hot spot regions, CT technique has been applied, which is a rule-based thresholding algorithm [25]. The mathematical expression of CT is shown in "(6)" and "(7)".

$$\text{Test 1: } \rho \le m_\rho \quad (6)$$

$$\text{Test 2: } \rho \ge [m_\rho - n(\sigma_\rho)], \text{ and } \rho \le [m_\rho - (n-1)\sigma_\rho] \quad (7)$$

Where, m_ρ is Median of the whole image, σ_ρ is the standard deviation of the whole image and ρ represent the NDVI image to be classify.

In this present study, to obtain the value of n, n is taken as 0.1 to 3.5, and with the interval of 0.1 it is increased to retrieve the highest detection accuracy. To evaluate the performance of CT, HDA and FAR are calculated. The detailed overview and the mathematical formulation of HDA and FAR are given in [25]. After carrying out the critical analysis of n on NDVI_03 image, it is observed that CT is producing the highest detection accuracy for the value of 3 and hence, for this study the value of n is taken as 3 which has been applied on the NDVI_03 image to retrieve the hot spot and non-hot spot regions with high HDA and less FAR. The resultant image is obtained as CT_ NDVI_03 and shown in Fig. 5.

C. Calculation of HDA and FAR to Evaluate the Performance of CT for Hot Spot and Non-hot Spot Regions

The ground truth information of hot spots present in JCF are used as the testing sample to test the classification accuracy of classified image. HDA and FAR from "(6)" and "(7)" have been measured for both the classified images and it is observed that CT is quite effectively and efficiently classified the hot spot and non-hot spot pixels of both the images. After apply the CT, HDA is obtained as 86.6% and FAR is obtained as 0.80%, which is highly acceptable to delineate the hot spot boundaries

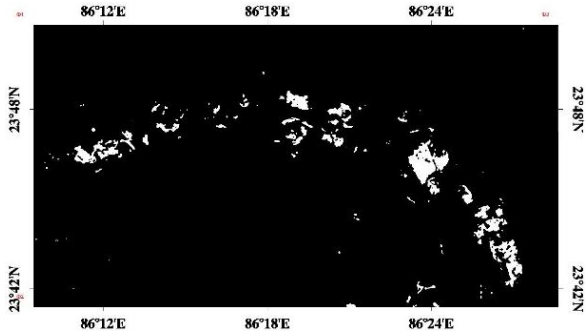

Fig. 5. Two class classified image of JCF region (i.e. CT_NDVI_03)

D. Testing of CT for Hot Spot and Non-hot Spot Regions

The CT algorithm has been applied on the January (i.e. IMG_01) and February (i.e. IMG_02) month's images to test the performance of the algorithm for the value of n (i.e. 3). NDVI images are calculated from IMG_01 and IMG_02 by using "(1)" and NDVI images are retrieved as NDVI_01 and NDVI_02, and shown in the Fig. 6 (a) and 6 (b).

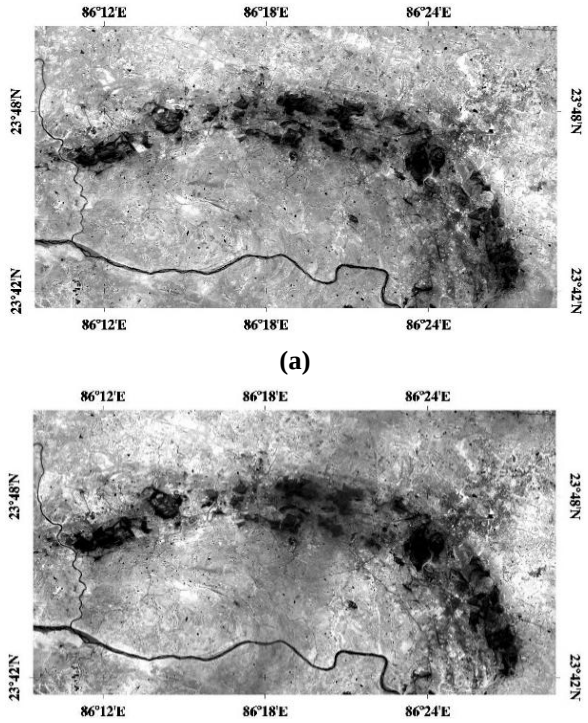

Fig. 6. NDVI images, (a) NDVI_01 and (b) NDVI_02

To test the performance of CT, the value of n is taken as 3 and it has been applied on NDVI_01 and NDVI_02 images to retrieve the hot spot and non-hot spot regions.

From both the images, HDA is retrieved as 75.41% and 77.54% respectively and FAR is retrieved as 3.32 and 3.16 respectively, and it is observed that these images are also acceptable to delineate the hot spot boundaries. The resultant images of contextual thresholding are obtained as CT_NDVI_01 and CT_NDVI_02, and shown in the Fig. 7 (a) and 7 (b).

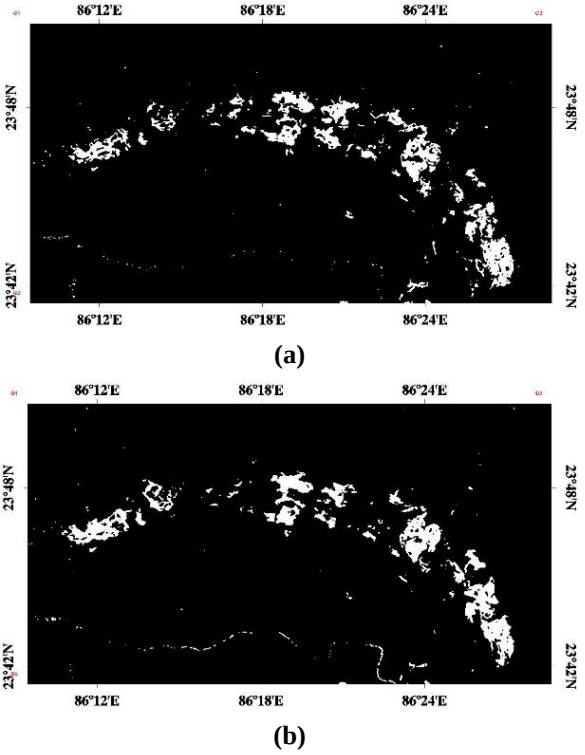

Fig. 7. Two class classified image of JCF region, (a) CT_NDVI_01 and CT_NDVI_02

E. Validation of CT for Hot Spot and Non-hot Spot Regions

April, May and June month's images have been taken to validate the performance of CT algorithm. For validation purpose, the value of n is taken as 3 and both the test were applied on to the obtained NDVI images. NDVI images are calculated from IMG_04, IMG_05 and IMG_06 by using "(1)" and are retrieved as NDVI_04, NDVI_05 and NDVI_06, and shown in the Fig. 8 (a), 8 (b) and 8 (c).

To validate the performance of the CT algorithm, the value of n is also taken as 3 and has been applied on NDVI_04, NDVI_05 and NDVI_06 images to retrieve the hot spot and non-hot spot regions. From the classified images, HDA is retrieved as 82.49%, 84.95%, and 81.21 respectively and FAR is retrieved as 3.03, 3.91, and 1.44 respectively, which are also altogether acceptable to delineate the hot spot boundaries. The resultant images of contextual thresholding are obtained as CT_NDVI_04, CT_NDVI_05 and CT_NDVI_06 and shown in Fig. 9 (a), 9 (b) and 9 (c).

F. Calculation of Sensitivity and Specificity to Evaluate the Performance of CT for Hot Spot and Non-hot Spot Regions

The performance of the detected hot spot pixels has been evaluated by computing the True Positive, False Positives, True Negatives and False Negatives pixels. True positives (TP) are hot spot pixels correctly labelled as positive pixels while False positives (FP) refer to the negative hot spot pixels incorrectly labelled as positive pixels. On the other hand, True negatives (TN) correspond to negative hot spot pixels correctly labelled as negative pixels, while False negatives (FN) refer to positive hot spot pixels incorrectly labelled as negative pixels [26]. After calculating the TP, FP, TN and FN pixels, to identify the correctly detected hot spot and non-hot spot pixels, two performance measures i.e. Sensitivity and Specificity are also estimated.

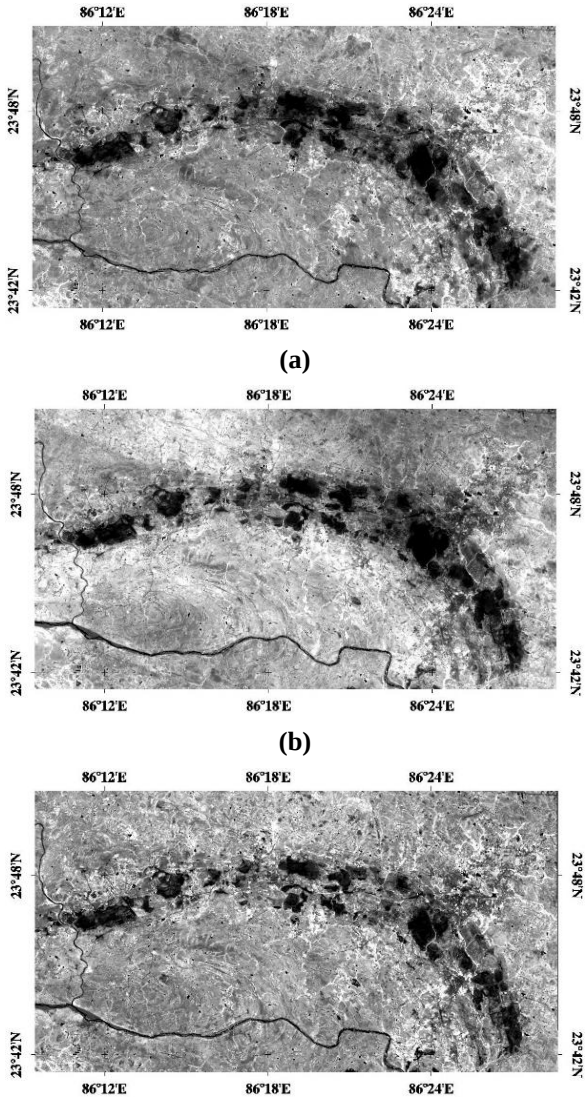

Fig. 8. NDVI images, (a) NDVI_04, (b) NDVI_5 and (c) NDVI_06

Sensitivity refers to the percentage of pixels correctly identified as hot spot pixels, while specificity refers to the percentage of pixels correctly identified as non-hot spot pixels.

Higher the value of Sensitivity and Specificity (closer to 1), more accurate will be the result. The comparative results of detected hot spot and non-hotspot of contextual algorithm in terms of Sensitivity and Specificity are shown in Fig. 10 (a) and 10 (b). The mathematical formulation of Sensitivity and Specificity are given in "(8)" and "(9)".

$$\text{Sensitivity} = \frac{TP}{TP + FN} \quad (10)$$

$$\text{Specificity} = \frac{TN}{TN + FN} \quad (11)$$

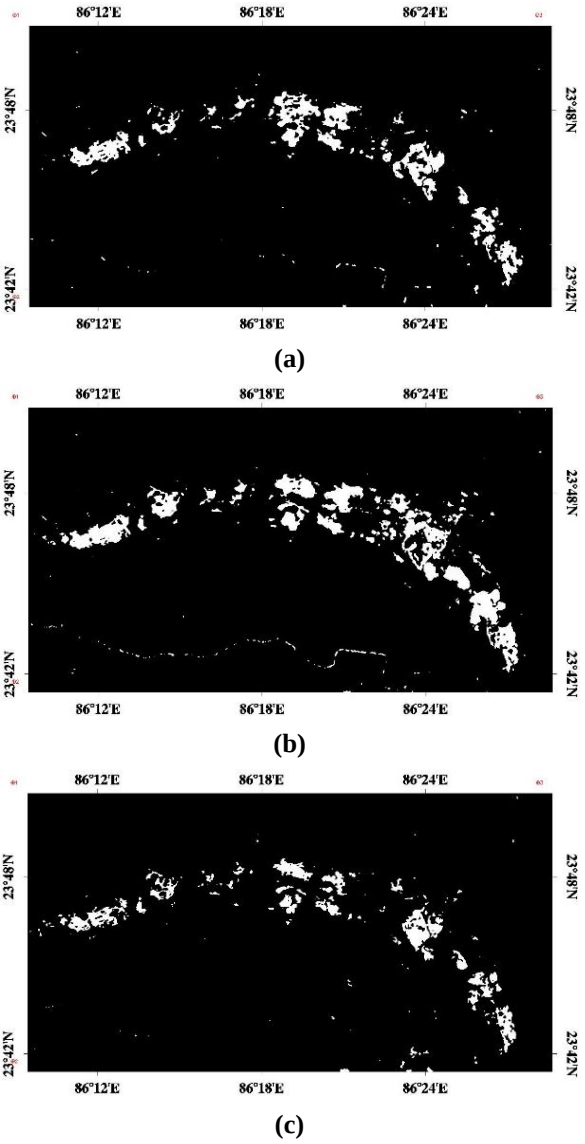

(a)

(b)

(c)

Fig. 9. Two class classified image of JCF region, (a) CT_NDVI_04, (b) CT_NDVI_05 and (c) CT_NDVI_06

From Fig. 10 (a) and 10 (b), it is observed that for all the six months Landsat-8 images CT is found to be much more specific for hot spot and not-hot spot regions and algorithm has shown the significant sensitivity. These results indicate that hot spots were detected accurately in a successful and efficient manner. It is also observed that the sensitivity and specificity are not constant for the different months and the obtained average value is quite satisfactory as shown in Fig. 10 (a) and 10 (b). The main reason behind this may be the variation in weather conditions in different months during the time of image acquisition.

G. Hough Transform on Hot Spot Detected Images

In this present study, the hot spot and non-hot spot pixels are classified by CT algorithm. Since the hot spot regions are the main region of interest, the non-hot spot regions composed of other regions such as vegetation, built-up areas, road and water bodies (Damodhar River valley). Therefore, in order to delineate the boundaries of the hot spot regions, Canny edge detection algorithm is applied to detect the edges of hot spot areas. Later, Hough transform is applied to vector image to detect the edges. From Fig. 10 (a), it is observed that March month image (i.e. CT_NDVI_03) is producing the high detection accuracy in comparison to other month's images. Other month images (i.e. CT_NDVI_01, CT_NDVI_02, CT_NDVI_04, CT_NDVI_05, and CT_NDVI_06) are also producing the high HDA, which is a very good detection accuracy and indicate that these images are also acceptable for Hough Transform based hot spot boundaries delineation.

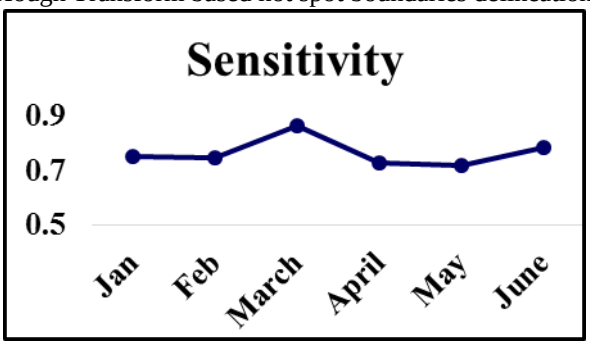

(a)

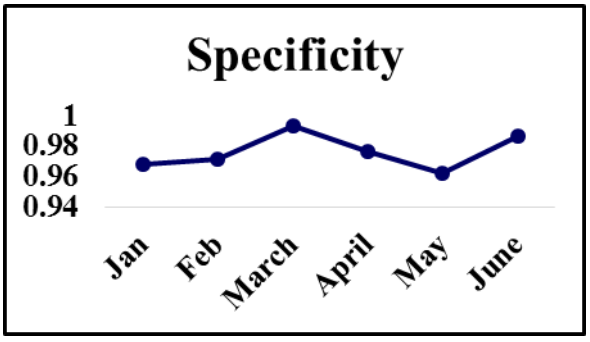

(b)

Fig. 10. Comparison of performance of contextual techniques in terms of (a) sensitivity and (b) specificity for detecting hot spots in 6 months images of JCF region.

After implementing the Hough transform, the delineated hot spot boundaries are shown in Fig. 11 (a), 11 (b), 11(c), 11(d), 11(e) and 11 (f), where it has been observed that the hot spot boundaries have been delineated effectively and efficiently. To assess the delineated hot spot boundaries, hot spot detection percentage has been measured which gives the percentage of hot spot areas appropriately extracted by the automatic process of Hough Transform and defines whether

the hot spot boundaries produced by automatic process is true or not. The hot spot detection percentage (HDP) is calculated as:

$$HDP = 100 \times TP(TP+FP+FN) \quad (10)$$

By using the "(10)", the BDP for NDVI_01, NDVI_02, NDVI_03, NDVI_04, NDVI_05, and NDVI_06 are retrieved as 65.22%, 74.95%, 86.64%, 73.03%, 72.24%, and 78.48% respectively. It is observed that proposed approach is quite effective for delineating the hot spot boundaries.

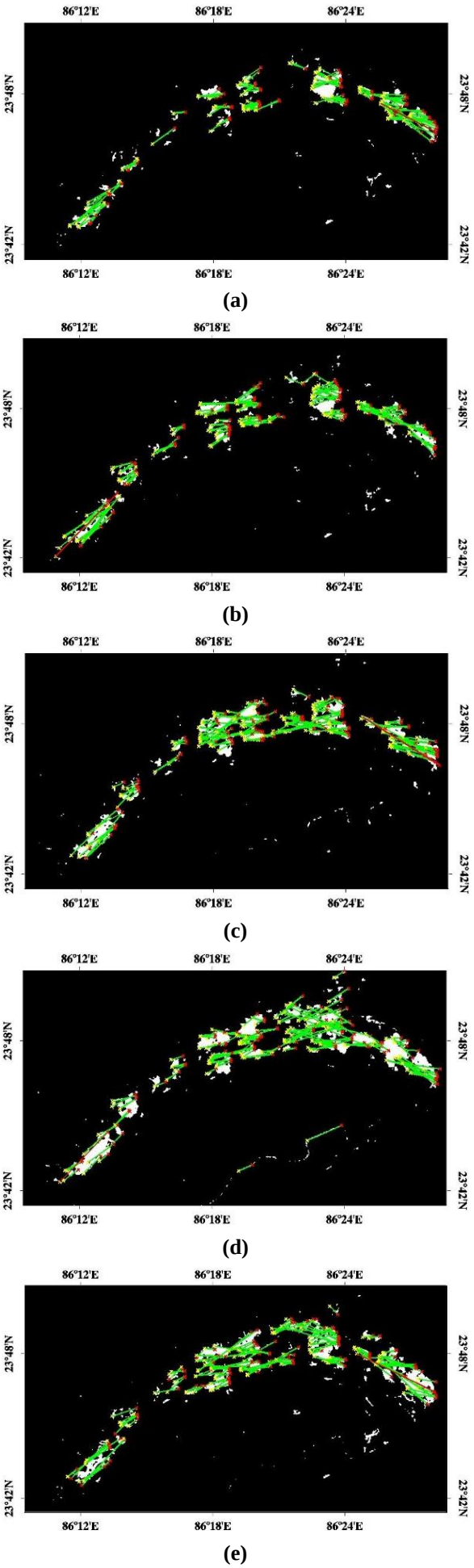

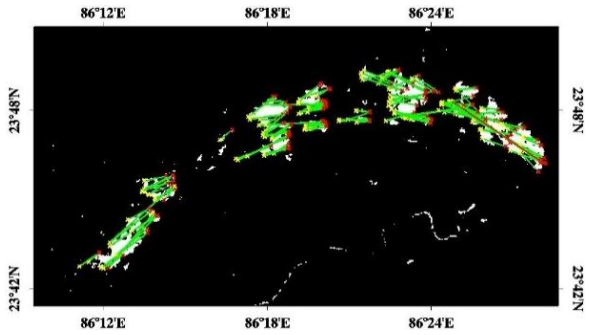

Fig. 11. Delineated hot spot boundaries of JCF region from (a) CT_NDVI_01, (b) CT_NDVI_02, (c) CT_NDVI_03, (d) CT_NDVI_04, (e) CT_NDVI_05 and, (f) CT_NDVI_06.

VI. CONCLUSION

The Jharia coal field is the undisputed premier storage facility of prime coke coal in the entire region of South-Asian peninsular. This zone has been seething with underground subsurface fires (i.e. hot spot) for a very long period of time. JCF contains almost 50% of the total hot spots in entire Indian coalfields. The main objective of this research work is to give a promising answer for the issue of hot spot monitoring by analyzing freely available satellite images. The proposed research then focuses on developing separate algorithms for hot spot detection by utilizing the advantages offered by enhancement techniques. In the first stage, the process of hot spots detection embark upon resultant images retrieved from CT based classification, which have shown all the six month's images classified with quite high detection accuracy and indicate that these images are highly acceptable for hot spot boundaries identification. In the second stage, the Canny edge detection algorithm is applied to detect the edges of the hot spot regions and then the binary image is generated, which is later converted into a vector image. Finally Hough transform is implemented on the classified images for delineating hot spots boundaries. The delineated hot spot boundaries can be used to obtain the expansion or shrinking information of hot spot regions. In future, the delineated boundaries may be utilized for hot spot area estimation, which can be used to develop a better and effective hot spot monitoring.

ACKNOWLEDGMENT

Authors are thankful to Integral University, Lucknow, India for supporting this work.

REFERENCES

1. V. Saini, R. P. Gupta, and M. K. Arora, "Environmental issues of coal mining-A case study of Jharia coal-field, India," in International Conference on Engineering Geology in New Millennium, At IIT Delhi, New Delhi. doi, 2015, vol. 10.
2. Tajdarul Hassan Syed, Moidu Jameela Riyas, and Claudia Kuenzer, "Remote sensing of coal fires in India: A review," Earth-Sci. Rev., vol. 187, pp. 338–355, 2018.
3. W. Schroeder, P. Oliva, L. Giglio, B. Quayle, E. Lorenz, and F. Morelli, "Active fire detection using Landsat-8/OLI data," Remote Sens. Environ., vol. 185, pp. 210–220, 2016.

4. H. Huo et al., "A Study of Coal Fire Propagation with Remotely Sensed Thermal Infrared Data," Remote Sens., vol. 7, no. 3, pp. 3088–3113, 2015.
5. A. Raju, R. P. Gupta, and A. Prakash, "Delineation of coalfield surface fires by thresholding Landsat TM-7 day-time image data," Geocarto Int., vol. 28, no. 4, pp. 343–363, 2013.
6. A. Prakash, R. P. Gupta, and A. K. Saraf, "A Landsat TM based comparative study of surface and subsurface fires in the Jharia coalfield, India," Int. J. Remote Sens., vol. 18, no. 11, pp. 2463–2469, 1997.
7. D. Coppola, M. Laiolo, D. Delle Donne, M. Ripepe, and C. Cigolini, "Hot-spot detection and characterization of strombolian activity from MODIS infrared data," Int. J. Remote Sens., vol. 35, no. 9, pp. 3403–3426, 2014.
8. C. Hecker, C. Kuenzer, and J. Zhang, "Remote-sensing–based coal-fire detection with low-resolution MODIS data," Geol. Coal Fires Case Stud. World Geol. Soc. Am. Rev. Eng. Geol., vol. 18, pp. 229–239, 2007.
9. A. Gautam, R. S. Gautam, and N. Saxena, "An intelligent wavelet transform-based framework to detect subsurface fires with NOAA–AVHRR images," Int. J. Remote Sens., vol. 33, no. 4, pp. 1276–1295, 2012.
10. R. S. Gautam, D. Singh, and A. Mittal, "An efficient contextual algorithm to detect subsurface fires with NOAA/AVHRR data," IEEE Trans. Geosci. Remote Sens., vol. 46, no. 7, pp. 2005–2015, 2008.
11. R. S. Gautam, D. Singh, and A. Mittal, "Detection of hotspots in NOAA/AVHRR images using principal component analysis and information fusion technique," Int. Arch. Photogramm. Remote Sens. Spat. Inf. Sci., vol. 36, no. 4, pp. 951–956, 2006.
12. S. H. Boles and D. L. Verbyla, "Comparison of three AVHRR-based fire detection algorithms for interior Alaska," Remote Sens. Environ., vol. 72, no. 1, pp. 1–16, 2000.
13. W. Chen, K. Moriya, T. Sakai, L. Koyama, and C. X. Cao, "Mapping a burned forest area from Landsat TM data by multiple methods," Geomat. Nat. Hazards Risk, vol. 7, no. 1, pp. 384–402, 2016.
14. Y. Xue, J. Liu, J. Li, C. Shang, J. Zhao, and M. Zhang, "Use of Landsat thermal imagery for dynamically monitoring spontaneous combustion of Datong Jurassic coalfields in China," J. Earth Syst. Sci., vol. 127, no. 4, p. 47, 2018.
15. A. Prakash, K. Schaefer, W. K. Witte, K. Collins, R. Gens, and M. P. Goyette, "A remote sensing and GIS based investigation of a boreal forest coal fire," Int. J. Coal Geol., vol. 86, no. 1, pp. 79–86, 2011.
16. R. S. Gautam, D. Singh, A. Mittal, and P. Sajin, "Application of SVM on satellite images to detect hotspots in Jharia coal field region of India," Adv. Space Res., vol. 41, no. 11, pp. 1784–1792, 2008.
17. D. K. San and M. Turker, "Building extraction from high resolution satellite images using Hough transform," Int. Arch. Photogramm. Remote Sens. Spat. Inf. Sci., vol. 38, no. Part 8, 2010.
18. V. Saini, R. P. Gupta, and M. K. Arora, "Environmental impact studies in coalfields in India: A case study from Jharia coal-field," Renew. Sustain. Energy Rev., vol. 53, pp. 1222–1239, 2016.
19. E. G. Cadau, A. Burini, C. Putignano, P. Goryl, and F. Gascon, "Multi-sensor rapid fire damage assessment over mediterranean area," in 34th International Symposium on Remote Sensing of Environment, 2011.
20. D. Stroppiana, S. Pinnock, J. M. Pereira, and J.-M. Grégoire, "Radiometric analysis of SPOT-VEGETATION images for burnt area detection in Northern Australia," Remote Sens. Environ., vol. 82, no. 1, pp. 21–37, 2002.
21. D. P. Argialas and O. D. Mavrantza, "Comparison of edge detection and Hough transform techniques for the extraction of geologic features," Int. Arch. Photogramm. Remote Sens. Spat. Inf. Sci., vol. 34, no. Part XXX, 2004.
22. H. Taud and J.-F. Parrot, "Detection of circular structures on satellite images," Int. J. Remote Sens., vol. 13, no. 2, pp. 319–335, 1992.
23. Y. Rianto, "Road network detection from SPOT satellite image using Hough transform and optimal search," in Asia-Pacific Conference on Circuits and Systems, 2002, vol. 2, pp. 177–180.
24. A. S. Hassanein, S. Mohammad, M. Sameer, and M. E. Ragab, "A survey on Hough transform, theory, techniques and applications," ArXiv Prepr. ArXiv150202160, 2015.
25. T. Ahmed, D. Singh, S. Gupta, and B. Raman, "An efficient application of fusion approach for hot spot detection with MODIS and PALSAR-1 data," Geocarto Int., vol. 31, no. 7, pp. 715–738, 2016.
26. D. D. Nagaveena and S. P. Kumar, "Vessels segmentation in diabetic retinopathy by adaptive median thresholding," Int. J. Sci. Technoledge ISSN 2321–919X, 2013.

AUTHORS PROFILE

Tasneem Ahmed received his PhD degree in 2016 in Image Processing from IIT Roorkee, India. Currently, he is working as an Assistant Professor in the Department of Computer Application, Integral University Lucknow, India. His research interests include digital image processing, optical and microwave satellite image processing, image classification, data fusion, time series analysis, and SAR data analysis for land cover classification.

Mohammad Usama received his M. Sc. degree in 2006 and M. Phil degree in 2008 in Environmental Sciences. Currently, he is working as an Assistant Professor in the Department of Environmental Science, Integral University Lucknow, India. His research interests include Organic Farming and Waste Management, Disaster Management, Insilico Toxicology, Bioremediation, Climate Change, Sustainable Development.